Nanoscale Advances

ROYAL SOCIETY OF CHEMISTRY

PAPER

View Article Online
View Journal | View Issue

Open Access Article. Published on 17 May 2021. Downloaded on 7/24/2024 3:29:31 PM.
This article is licensed under a Creative Commons Attribution 3.0 Unported Licence.

Check for updates

Cite this: *Nanoscale Adv.*, 2021, **3**, 3816

Glucose oxidase kinetics using MnO_2 nanosheets: confirming Michaelis–Menten kinetics and quantifying decreasing enzyme performance with increasing buffer concentration†

Mahip Singh,‡[a] Ungku Zoe Anysa Ungku Faiz,‡[a] Steven Gravelsins,[a] Yoshinori Suganuma,[a] Nicholas Konstantine Kotoulas,[a] Mark Croxall,[a] Ahlia Khan-Trottier,[b] Cynthia Goh[a] and Al-Amin Dhirani *[ac]

Received 27th April 2021
Accepted 16th May 2021

DOI: 10.1039/d1na00311a

rsc.li/nanoscale-advances

MnO_2 nanosheets and ultraviolet-visible (UV-Vis) absorbance spectroscopy are used to study glucose oxidase (GOx) kinetics. Glucose oxidation by GOx produces H_2O_2, which rapidly decomposes the nanosheets and reduces their absorption. This direct approach for monitoring glucose oxidation enables simpler, real time kinetics analysis compared to methods that employ additional enzymes. Using this approach, the present study confirms that GOx kinetics is consistent with the Michaelis–Menten (MM) model, and reveals that the MM constant increases by an order of magnitude with increasing buffer concentration. Since larger MM constants imply higher enzyme substrate concentrations are required to achieve the same rate of product formation, increasing MM constants imply decreasing enzyme performance. These results demonstrate the facility of using MnO_2 nanosheets to study GOx kinetics and, given the widespread applications of enzymes with buffers, the important sensitivity of enzyme–buffer systems on buffer concentration.

1. Introduction

Manganese dioxide (MnO_2) can be used for a variety of applications such as biosensing in biomedical applications,[1] energy storage in batteries,[2] water decontamination at low temperatures,[3] catalysis with high activity and thermal stability,[4] and hydrogen peroxide decomposition to oxygen and water.[5] Recently, studies have reported that aqueous solutions of MnO_2 nanosheets can be easily synthesized according to Scheme 1.[6] Nanosheets are characterized by nanometre-scale (potentially atomic-scale) thicknesses and micrometre-scale lateral dimensions.[6] Other materials that can be isolated as nanosheets include graphite, molybdenum disulphide and boron nitride.[7] Increasing recent interest in such nanosheet forms of materials has arisen due to significant differences in chemical and physical properties exhibited by nanosheets compared to their bulk counterparts; for example, nanosheets possess much higher specific surface areas and can even exhibit distinct band structures and spectral behaviour. MnO_2 nanosheets, for example, exhibit a prominent ultraviolet-visible (UV-Vis) spectral peak around 386 nm.[6] Recent studies have reported that the peak decreases in the presence of H_2O_2 as H_2O_2 acts as an oxidizing agent[6] and rapidly decomposes the nanosheets as per Scheme 2.[8,9] This spectral behaviour suggests a potential application for monitoring glucose oxidation since H_2O_2 is a product of this reaction, as seen in Scheme 3.[9] Potential biological and medical applications include detecting H_2O_2 in cells and monitoring health/detecting diseases[10] in low resource environments.[9,11]

MnO_2 nanosheets also potentially provide a new tool for studying glucose oxidase (GOx) kinetics in real time. As per Scheme 3, GOx catalyzes oxidation of glucose and the production of H_2O_2, which can be monitored *via* MnO_2 decomposition in real time using UV-Vis spectroscopy. The present study confirms that this is possible and finds that the reaction

$$TMA \cdot OH + MnCl_2 + H_2O_2 \rightarrow MnO_2\ nanosheets$$

(TMA = Tetramethylammonium)

Scheme 1

$$MnO_2 + H_2O_2 + 2\ H^+ \rightarrow Mn^{2+} + 2\ H_2O + O_2$$

Scheme 2

[a]Department of Chemistry, University of Toronto, Ontario, Canada, M5S 3H6. E-mail: a.dhirani@utoronto.ca

[b]Department of Biochemistry, University of Toronto, Ontario, Canada, M5S 3H6

[c]Department of Physics, University of Toronto, Toronto, Ontario, Canada, M5S 3H6

† Electronic supplementary information (ESI) available. See DOI: 10.1039/d1na00311a

‡ These authors contributed equally.

© 2021 The Author(s). Published by the Royal Society of Chemistry

Open Access Article. Published on 17 May 2021. Downloaded on 7/24/2024 3:29:31 PM.
This article is licensed under a Creative Commons Attribution 3.0 Unported Licence.

$$Glucose + O_2 \xrightarrow{GOx} H_2O_2 + gluconic\ acid$$

Scheme 3

between MnO_2 and H_2O_2 occurs more rapidly than that of glucose oxidation. A resulting advantage of using this approach is that analysis of GOx kinetics is greatly simplified compared to approaches that employ additional enzymes, such as horseradish peroxidase (HRP), to detect H_2O_2 by a colour change.[12] Previous studies have reported other methods for quantifying H_2O_2, for example, using composite materials and electrochemistry or conductivity measurements.[13,14] However, application of these methods to study GOx kinetics has not been demonstrated.

Understanding enzyme kinetics is important as enzymes are common biocatalysts and are widely used in industrial processes.[15–19] GOx is an ideal candidate for studying enzyme kinetics given its stability and the ease of the method presented here.[12] Further, GOx itself has been used in a range of applications such as detecting and managing diabetes *via* glucose monitors functionalized with HRP,[11,12] modifying dairy texture,[20] and removing glucose from eggs to extend shelf-life.[21] We apply the present approach to monitor GOx kinetics in real time and test the applicability of the Michaelis–Menten (MM) kinetics model to GOx. We find that plots of initial rate *vs.* initial glucose concentration fit well to predictions of this model. We also confirm a hypothesis that GOx kinetics is affected by buffer concentration by measuring MM constants over a wide range of buffer concentrations. Enzyme activity is known to be affected by pH, and hence buffers are widely used to maintain constant pH. At the same time, the total ion concentration in solution will affect charge screening, protein structure and enzyme–substrate interactions; thus, the presence and concentration of the buffer itself, which alters the ion concentration of the solution, will have an effect on enzyme activity. For example, polar media are known to disrupt protein structure and influence protein function, as shown previously, and are expected to affect enzyme activity.[22] This has significant implications given ubiquitous applications of enzyme–buffer systems; however, the systematic quantification of any potential effects of buffer concentration on the function of enzymes has not been documented in the literature.

2. Experimental

Chemicals

Chemicals are purchased from Sigma Aldrich, Millipore, Fluka and ACP Chemicals. All chemicals were used as received. Deionized- (DI-) water is obtained in-house (18.2 MOhm cm^{-1} at 25 °C).

Synthesis, purification and isolation of MnO_2 nanosheets

MnO_2 nanosheets are synthesized using published methods.[6,9] 2.0 mL of H_2O_2 (30% by weight in water, ACS Grade, Sigma Aldrich, 216763 500 mL bottle) is added to 3.94 mL of aqueous tetramethylammonium hydroxide (TMA·OH, 25% by weight in water, Sigma Aldrich, 331635 250 mL bottle) in 14.1 mL of H_2O. This mixture is added within 15 seconds to 0.2845 g of aqueous manganese chloride, $MnCl_2$ (≥99%, trace metal basis, Sigma Aldrich 244589 10 g bottle) in 10.0 mL of water. The mixture exhibits effervescence for roughly 5 minutes and becomes a dark brown suspension. The mixture is stirred overnight at room temperature in air and can be stored in a refrigerator before further processing.

To remove larger particles, the suspension is sonicated (Branson 1510 sonicator) for 2 hours and centrifuged at ~3000 rpm for 40 minutes. The supernatant is then vacuum filtered and, to facilitate washing, its volume is reduced to ~5 mL by heating to 73 °C and vacuum pumping using a rotary evaporator. The nanosheets in solution are precipitated by adding 10 mL ethanol (95% in water) and centrifuging for 20 minutes at ~3000 rpm. The precipitate is washed with ethanol and redispersed in DI-water. The precipitation and washing steps are repeated using 20 mL ethanol and centrifuging for 30 minutes. The supernatant is removed, leaving behind a small amount of brown viscous precipitate. The precipitate, which contains the MnO_2 nanosheets, is washed again with methanol and stored at 5 °C under argon in a parafilm-sealed vial. To test reproducibility, the synthesis is performed twice, and products from both syntheses are used in kinetic measurements reported below.

Kinetic measurements

MnO_2 nanosheet solutions are freshly prepared from precipitate on the same day that kinetic measurements are performed. 0.0075 g of MnO_2 precipitate is dispersed in 20 mL DI-water, sonicated for ~20 minutes and centrifuged for ~25 minutes. The supernatant containing nanosheets is transferred to a clean vial, and the precipitate is discarded. The nanosheet solution is diluted as needed to ensure the absorbance at the beginning of each kinetic measurement is approximately 0.9. Various stock solutions are prepared and diluted as needed: 19.52 g of 2-(*N*-morpholino)ethane sulfonic acid (MES buffer, ULTROL grade, Millipore 475893, 100 g bottle) in 80 mL of DI-water, 0.0075 g of GOx (from *Aspergillus niger*, ~135 U mg^{-1}, Sigma Aldrich G7141) in 1.0 mL of DI-water, and 40 mM of β-D-glucose (>99%, HPLC grade, Fluka Biochemika) in DI-water. The DI-water is exposed to ambient atmosphere to allow oxygen diffusion. MES buffer and glucose (with concentrations as described below) as well as MnO_2 nanosheets (diluted as needed to ensure an initial absorbance of ~0.8–1.0 at 384 nm) are combined in a quartz cuvette for UV-Vis spectroscopy (Lambda 25 UV/Vis Spectrometer). The spectrometer's lid is opened after 30 seconds to inject GOx, the solution is stirred at the start of each kinetic run, and then the lid is closed. A cardboard covered in black electrical tape is used as a homemade cover to reduce ambient light reaching the spectrometer's detector while the spectrometer's lid is open. The homemade cover has a hole cut to allow access to the cuvette and is left in place throughout the kinetic run.

Nanosheet characterization

MnO_2 nanosheets are imaged using scanning electron microscopy (SEM, Hitachi S-5200, operated at 5.0 kV) and atomic force

Open Access Article. Published on 17 May 2021. Downloaded on 7/24/2024 3:29:31 PM.
This article is licensed under a Creative Commons Attribution 3.0 Unported Licence.

microscopy (AFM, JPK Nanowizard II, tapping mode). Energy dispersive spectra (EDS) were obtained using an ESEM (FEI Quanta FEG 250) operated in high vacuum mode at 10 keV. Samples for SEM are prepared by sonicating nanosheets in water, diluting and drop-casting the solution onto Carbon Type-A TEM grids and drying the grids in air. Samples for AFM are prepared by drop-casting nanosheet solution on freshly cleaved mica and drying under ambient conditions (30% humidity) overnight for imaging the following day. These samples are imaged using a silicon cantilever (NCHR-20, NanoWorld) with a force constant of 40 N m^{-1}. The integral and proportional gains are set to 10 and 0.002, respectively.

3. Results and discussion

SEM and AFM images of nanosheets are shown in Fig. 1a–c. SEM images in Fig. 1a and b show that the nanosheets can be multi-layered, and that their lateral size is micron in scale. The nanosheets can appear as aggregates (Fig. 1a) potentially generated by drop-casting and drying steps. AFM images (Fig. 1c) exhibit steps and confirm that the nanosheets can be multilayered.[9] The height profile indicates that the thickness of each layer is ~1.2–1.5 nm, and the total thickness of the multilayer shown is ~3.5 nm. For comparison, a previous study[6] reported a value of 1.02 nm for the thickness of a MnO_2 monolayer. Fig. 1d shows a UV-Vis absorbance spectrum of nanosheets in DI-water. UV-Vis spectra consistently exhibit absorption over a broad range of wavelengths and a peak around 375–382 nm, which can be ascribed to d–d transitions[6] in Mn ions as previously reported. Previous studies[8,9] have also reported that nanosheet absorbance in this wavelength range decreases in the presence of H_2O_2 in direct proportion to the amount of H_2O_2. ESEM images are shown in Fig. 2a and S2.† Complementary EDS spectra taken at two locations shown in Fig. 2a. Characteristic Mn peaks appear at 5.9 eV (Kα) and 0.637 eV (Lα) and confirm the presence of Mn in the sample (Fig. 2b and S3†). Al peaks can be attributed to a sample holder and C peaks to a TEM grid.

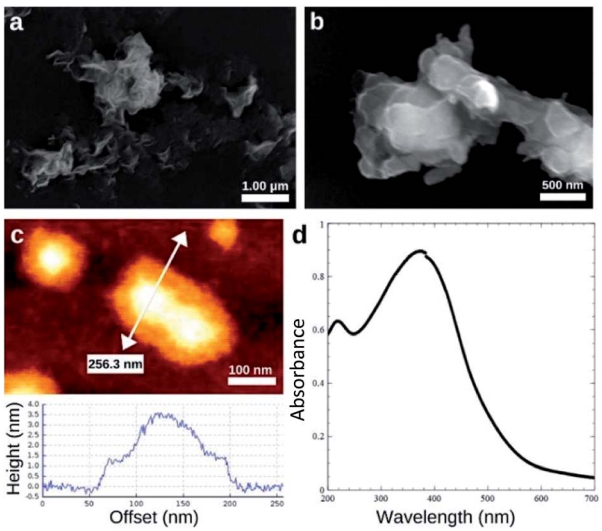

Fig. 1 Characterization of MnO_2 nanosheets. (a) Low and (b) high resolution SEM images. (c) AFM image obtained in tapping mode and height profile across the line shown. (d) UV/Vis spectrum of MnO_2 nanosheets in water.

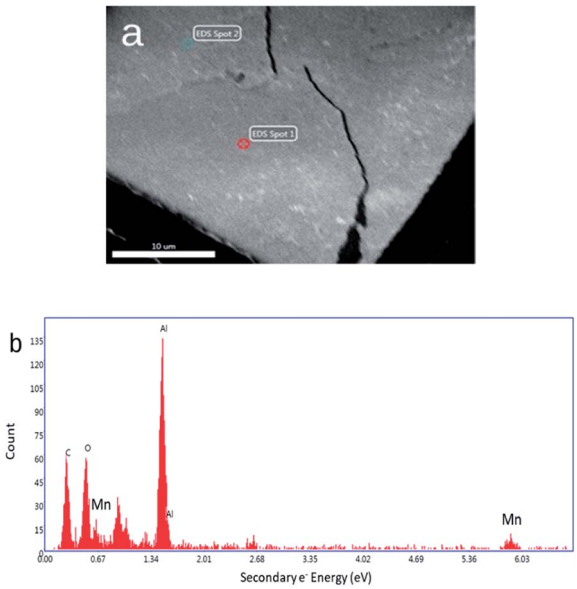

Fig. 2 (a) ESEM image of a thick MnO_2 film. (b) Energy dispersive spectrum obtained at Spot 1 shown in Fig. 2a (a spectrum obtained at Spot 2 is shown in Fig. S3†).

Fig. 3a pictures a general overview of changes in nanosheet colour in a variety of solutions with or without H_2O_2. Fig. 3a(1) shows a nanosheet solution in deionized water (relatively concentrated here for improved visibility), and Fig. 3a(6) shows a solution with the same nanosheet concentration 15 min after adding H_2O_2. The H_2O_2 causes a clear loss of colour. Fig. 3b shows a time evolution of a drop in absorbance of diluted nanosheet solution at 384 nm upon adding H_2O_2. The absorbance of the nanosheets drops significantly and rapidly upon addition of the H_2O_2. This serves as an important control test because glucose oxidation proceeds more slowly (the rates are discussed below). The nanosheet concentration is typical, and the 10 mM H_2O_2 concentration used for this test is an effective upper bound for the maximum possible H_2O_2 concentration available in any kinetic measurement performed in this study. Therefore, the rate-limiting step is the glucose oxidation reaction, and measurements of absorbance of nanosheets can be used as a straightforward means for analyzing kinetics for this reaction.

To ensure that MnO_2 absorption measurements accurately reflect GOx kinetics, stability tests are also conducted by combining various other relevant chemical species and MnO_2 nanosheets. Fig. 3a(3) shows that adding 1 mL of 1 M NaCl to a solution of MnO_2 and DI-water causes MnO_2 to precipitate (see inset), while Fig. 3a(2) shows that adding 1 mL of 1 M hydrogen chloride, HCl (36.5–38%, ACS Grade, ACP Chemicals H-6100) does not. The stability of MnO_2 in DI-water (pH 7) and in HCl (pH 0) indicates that the precipitation in Fig. 3a(3) can be attributed to Na^+ ions. Previous studies[23] have reported that

 © 2021 The Author(s). Published by the Royal Society of Chemistry

Open Access Article. Published on 17 May 2021. Downloaded on 7/24/2024 3:29:31 PM.
This article is licensed under a Creative Commons Attribution 3.0 Unported Licence.

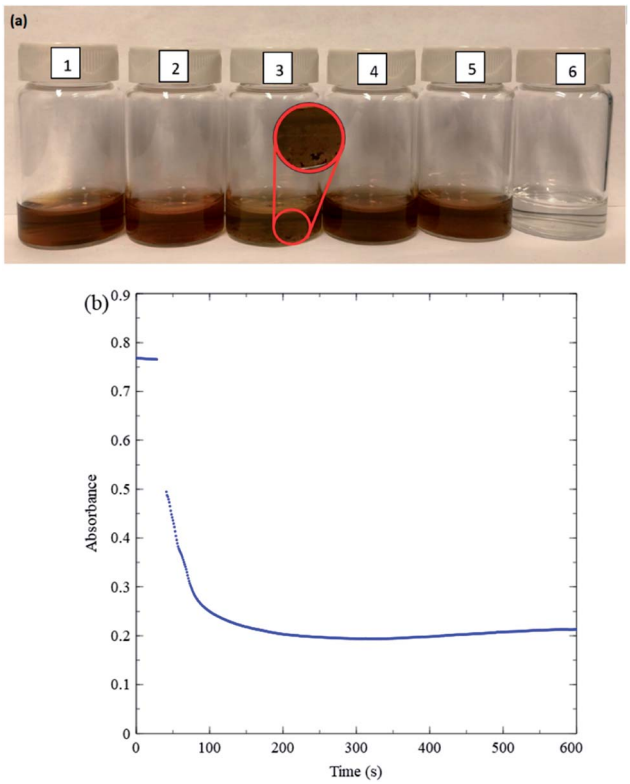

Fig. 3 (a) Photographs of various nanosheet solutions in DI-water 15 min. after preparation (1) MnO_2; (2) MnO_2 and HCl; (3) MnO_2 and NaCl; (4) MnO_2, MES buffer and glucose; (5) MnO_2, MES buffer, and gluconic acid; (6) MnO_2, MES buffer, gluconic acid and H_2O_2. (b) Absorbance of the nanosheets in DI-water at 384 nm *vs.* time upon injecting H_2O_2. Near the ~30 s mark, about 15 s of data have been omitted due to absorbance fluctuations caused by opening the spectrometer lid, injecting H_2O_2 and stirring. Initial reaction rate approx. 0.022 s^{-1}.

nanosheets can possess negative charges caused by Mn vacancies. We speculate that metal cations cause precipitation by interacting with such negative charges, in turn generating inter-nanosheet attraction. Precipitation is observed also when high concentrations (over 150 mM) of sodium phosphate buffer of pH 6.60–6.80 (Sigma Aldrich P8165) are added to MnO_2 and DI-water, likely for the same reason. Accordingly, only low concentrations of phosphate buffer are used for kinetic measurements in the present study. MES buffer (a Good's buffer) yields more stable MnO_2 solutions even at high buffer concentrations and is used for kinetic measurements over a wider range of buffer concentrations. Solutions with MnO_2 and MES buffer in DI-water continue to remain stable upon addition of glucose (Fig. 3a(4)) or gluconic acid (49–53% by weight in water, Sigma Aldrich G1951 1 kg bottle) (Fig. 3a(5)). The range of pH over which MnO_2 is stable includes values at which blood tests are conducted, around 5.8–7.4.[24]

Fig. 4 shows kinetic data varying GOx volume and initial MnO_2 concentration. Fig. 4a shows 384 nm absorbance of MnO_2 nanosheets *vs.* time for various GOx volumes keeping initial MnO_2 absorbance fixed (close to 0.9). In all trials, the total solution volume is 4 mL. GOx is injected at about the 30 s mark, and the solution is stirred for 10–15 seconds. Final GOx concentrations range from 0 to 150 mM after mixing. There is a high density of data points initially, so in order to discern slopes more easily, the inset in Fig. 4b plots initial kinetic data, after fitting a straight line and removes respective offsets. Fig. 5b is analyzed similarly. The slopes (*i.e.* initial rates) are plot in the main panel. Fig. 4b shows that the initial rates *vs.* GOx volume exhibits a linear relationship (linear correlation coefficient, $R^2 = 0.939$) consistent with the Michaelis–Menten model, as discussed further below. Subsequent kinetics measurements employed a GOx concentration that is midway in the range shown. It should be noted that there is a steady background decline in absorbance even when no GOx is added. However, this background decay occurs at a constant rate which is less than 2×10^{-4} s^{-1}, *i.e.* 10–15 times smaller than the rates obtained for the Michaelis–Menten experiments where GOx concentration is fixed and glucose concentration is varied (see

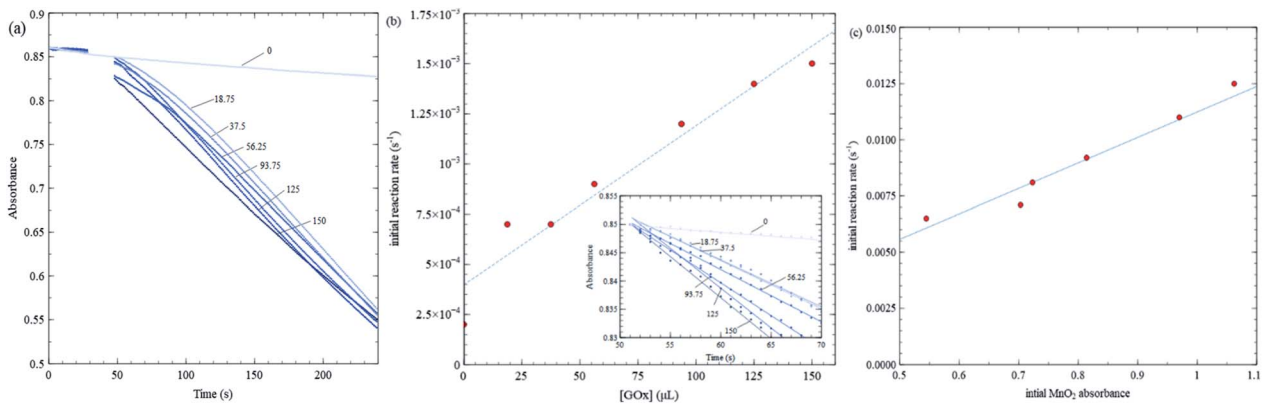

Fig. 4 Dependence of initial rate on volume of GOx injected into a 4 mL solution in a UV-Vis cuvette, keeping nanosheet, glucose and MES buffer concentrations fixed (nanosheet concentration using the absorbance, [glucose] = 0.5 mM, [MES] = 100 mM, [GOx] = 7.5 mg mL^{-1} concentrate before injection). (a) Absorbance at 384 nm *vs.* time for various volumes of GOx injected. GOx is injected at the 30 s mark and stirred. The label for each data set indicates volume (μL) of GOx solution injected. (b) Initial reaction rate *vs.* volume of GOx injected; the plot in (b) is obtained using data shown in (a), data translated to start at the same absorbance for clarity. (c) Initial reaction rate *vs.* MnO_2 absorbance and a linear fit.

Open Access Article. Published on 17 May 2021. Downloaded on 7/24/2024 3:29:31 PM.
This article is licensed under a Creative Commons Attribution 3.0 Unported Licence.

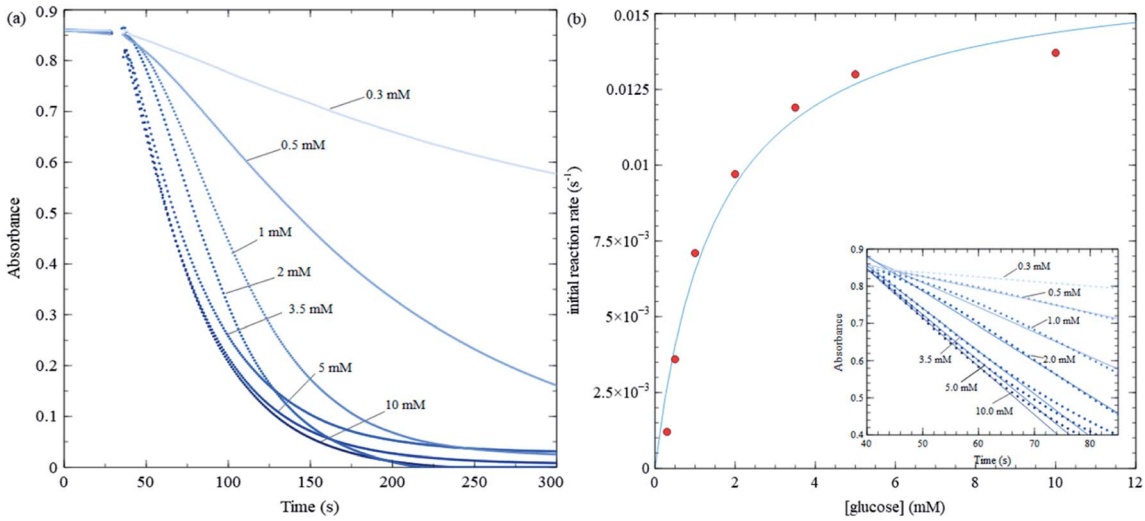

Fig. 5 Michaelis–Menten trial with varying glucose concentration, while keeping MES buffer, GOx and nanosheet concentrations fixed. (a) Absorbance at 384 nm *vs.* time for various glucose concentrations. (b) Initial reaction rate *vs.* glucose concentration for data shown in (a), along with a least square fit to eqn (1). The fitting yield 75 μL of 7.5 mg mL^{-1} GOx is injected into a 4 mL solution in a UV-Vis cuvette at the 30 s mark and stirred.

Fig. 5); hence, this background decay should not have a significant effect on the results concerning enzyme kinetics.

Fig. 4c shows initial rates for various MnO_2 concentrations keeping all other quantities fixed. The data exhibit a linear trend, indicating the rate is first order in MnO_2 concentration.

Fig. 5 shows kinetic data for several glucose concentrations from 0.1 mM to 10 mM, keeping MES buffer, GOx and MnO_2 concentrations fixed. These data show that the reaction in Scheme 2 proceeds more rapidly than that in Scheme 3, and hence, changes in nanosheet absorbance can be effectively used to measure H_2O_2 production and GOx reaction rates. The initial reaction rate for the control test in Fig. 3b is about 0.022 s^{-1}, while the fastest reaction rate over all MM trials is approximately 0.015 s^{-1}. The former is sufficiently fast that a significant portion of the reaction occurs during the initial stirring period. Also, in the control test, nanosheets react with the maximum concentration of H_2O_2 that is injected at one time, while during MM trials, the nanosheets react with H_2O_2 that is produced continuously and much more slowly.

Initial rates in Fig. 5 increase (slopes become steeper) as glucose concentrations increase; however, the increases are much more pronounced at lower glucose concentrations compared with higher concentrations. The MM model predicts that the initial rate (v) *vs.* substrate concentration ([S]) follows the following relation:

$$v = \frac{V_{\max}[\mathrm{S}]}{K_{\mathrm{m}} + [\mathrm{S}]} \tag{1}$$

where $V_{\max}$ and K_{m} are independent of [S]. $V_{\max} = k_{\mathrm{cat}}[\mathrm{E}]_0$ is the maximum initial rate achieved at high substrate concentration, k_{cat} is the catalytic rate constant to produce product (P in Scheme 4), and $[\mathrm{E}]_0$ is the enzyme concentration. Consistent with Fig. 4b, $V_{\max}$ is proportional to enzyme concentration according to the model, as mentioned. K_{m} is the substrate concentration at which $v = \frac{1}{2}V_{\max}$ and is a measure of enzyme performance: higher K_{m} values indicate lower performance since higher substrate concentrations are required to achieve $v = \frac{1}{2}V_{\max}$. Eqn (1) predicts that the initial rate increases linearly at low [S], when enzyme is available, and saturates to $V_{\max}$ at high [S], when total enzyme activity becomes a bottleneck for the reaction. Fig. 5b shows initial rates *vs.* glucose concentration, where the initial rates are calculated by linear fits to data in Fig. 5a over a 30–60 second duration following enzyme addition. Also shown is a fit to these data using eqn (1). Trends in the data are in good agreement with the MM model, both at low and high glucose concentrations.

As an application of the present method, we study enzyme kinetics at different buffer concentrations (all with pH ∼ 5.8) to explore any potential influence of buffer concentration on enzyme–substrate interactions. Fig. 6 summarizes the results obtained over 16 mM trials using MES buffer and nanosheets from two syntheses, phosphate buffer at low buffer concentrations and no buffer. Although the no buffer values provide a consistency check, they are expected to be less reliable due to changing enzyme activity caused by changing pH. As an independent consistency test, we also study kinetics at zero buffer concentration using a conductivity meter and include the results in Fig. 6. Production of gluconic acid (*i.e.* H^+ ions, which are very mobile) produces a change in conductivity that is easily detected using a conductivity meter when background ion concentration is low (see Scheme 2 and Fig. S1 in ESI†). Fig. 6a shows a plot of K_{m} *vs.* buffer concentration. A straight line fit to

$$\mathrm{E} + \mathrm{S} \rightleftharpoons ES \rightarrow P$$

Scheme 4

 © 2021 The Author(s). Published by the Royal Society of Chemistry

Open Access Article. Published on 17 May 2021. Downloaded on 7/24/2024 3:29:31 PM.
This article is licensed under a Creative Commons Attribution 3.0 Unported Licence.

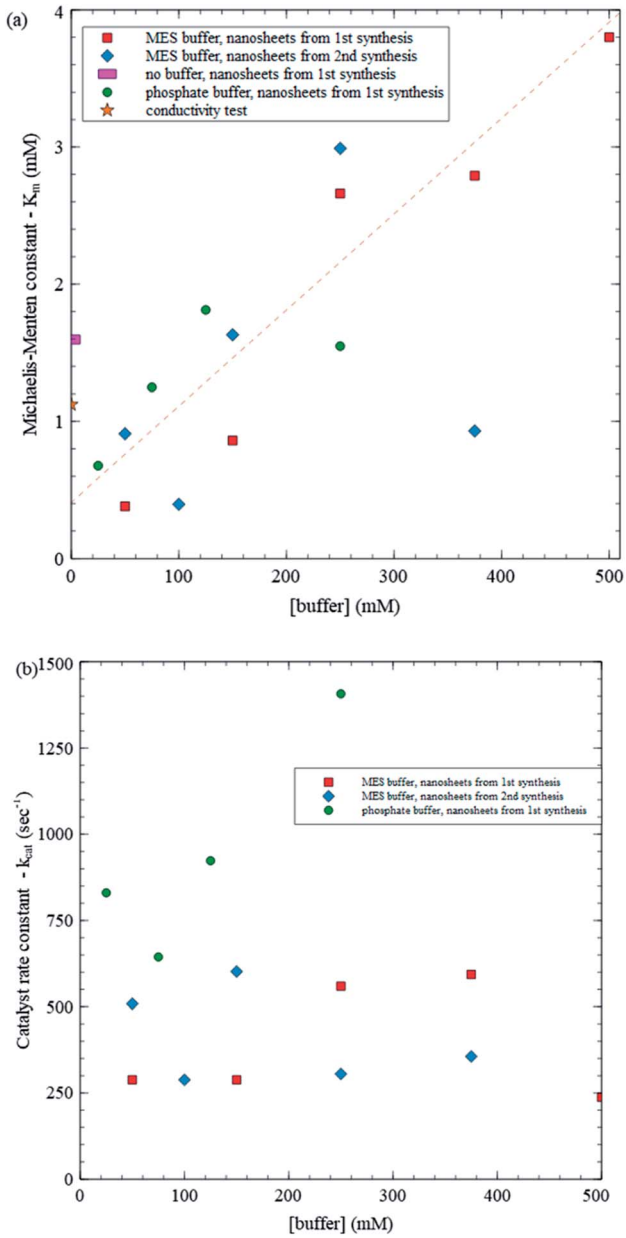

Fig. 6 (a) Michaelis–Menten constant (K_m) *vs.* buffer concentration, (b) catalyst rate constant (k_{cat}) *vs.* buffer concentration.

the data, excluding a point with $K_m \approx 1$ mM at 375 mM buffer concentration and the points with no buffer, yields a reasonably good fit with $R^2 = 0.801$ and $\sigma_{rms} = 0.467$, where σ_{rms} is the root mean square deviation from the fit. σ_{rms} provides a reasonable measure of variations within the data. Variations in K_m using (1) MES buffer and nanosheets from a given synthesis, (2) MES buffer and nanosheets from different syntheses and (3) different types of buffers (MES *vs.* phosphate) are all comparable to σ_{rms}, while the excluded data point is 4.5 σ_{rms} from the fit suggesting that it is an outlier. As the buffer concentration increases from 20 mM to 500 mM, the trendline indicates that K_m increases from 0.5 mM to 3.9 mM, *i.e.* by about an order of magnitude. The large increase is over 7 times σ_{rms} indicating that it statistically significant. There is some variation between the results from the two syntheses, but it is similar to the variation within each synthesis. After removing the outlier, the σ_{rms} for MES synthesis 1, MES synthesis 2 and phosphate buffer are 0.35, 0.41 and 0.308 respectively, all comparable to the overall σ_{rms} of 0.467.

Using the V_{max} values from the same trials, we can determine k_{cat} values as well (Fig. 6b). In contrast with K_m, k_{cat} does not exhibit a clear variation with buffer concentration: all points except one are within about one σ_{rms} (313 s^{-1}) from the average (559 s^{-1}). Combined, these results provide some insight into how varying buffer concentration affects enzyme kinetics. According to the MM model,

$$K_m = \frac{k_{-1} + k_{cat}}{k_1}$$

where k_1 and k_{-1}, respectively, are the rate constants for the forward and reverse reactions of the enzyme + substrate $\leftrightharpoons$ enzyme–substrate complex reaction (Scheme 4). In order for K_m to increase while k_{cat} remains constant with increasing buffer concentration, the enzyme–substrate complex should decompose back to reactants more quickly (k_{-1} increases) and/or the enzyme–substrate complex should form more slowly (k_1 decreases).

As mentioned, trends in K_m and k_{cat} with buffer concentration have not been reported in the literature. Reported values of K_m range widely across various studies from just under 10 to over 100 mM, and k_{cat} values vary between 100 to 1000 s^{-1}.[25–31] Reported K_m values are about an order of magnitude larger than those found in the present study and vary over an order of magnitude. Fig. 6a shows that differences in buffer can lead to large variations in values of K_m, suggesting that this may contribute to variations in reported values of K_m and that significantly lower K_m (and correspondingly higher enzyme performance) can be achieved depending on the buffer. Interestingly, k_{cat}, values found here are similar in magnitude to reported values, which is consistent with k_{cat} not exhibiting a systematic variation with buffer concentration.

The use of MnO_2 nanosheets enables a straightforward analysis of GOx kinetics and yields good agreement between the observed kinetics and the MM model. It also enables exploring the influence of varying buffer concentration. Previous studies have reported that buffer concentration has an effect on protein and enzyme structures, causing them to denature.[32] Given such denaturing (and potentially also interference with binding to other species, or mechanisms for degrading operation), loss of function can be anticipated in environments with high ion concentration. The present results suggest that similar adverse effects can be anticipated for buffer–enzyme combinations as well. To our knowledge, this is the first study to quantify a large, linear increase in K_m, indicating degrading function, with increasing buffer concentration using GOx as a test bed. These results are significant because they suggest that, whereas having some buffer is desirable to keep pH and enzyme activity stable, a minimum of buffer should be used to prevent significant adverse impact on enzyme performance.

Open Access Article. Published on 17 May 2021. Downloaded on 7/24/2024 3:29:31 PM.
This article is licensed under a Creative Commons Attribution 3.0 Unported Licence.

4. Conclusions

Decomposition of MnO_2 nanosheets by H_2O_2 and UV-Vis real time spectroscopy are used to study GOx kinetics. The study finds that GOx kinetics follows the MM model. Also K_m increases approximately linearly by about an order of magnitude with increasing buffer concentration. These results demonstrate the facility of the present method for studying GOx kinetics, and the strong adverse effect of high buffer concentrations on GOx and potentially other enzyme-catalyzed reactions.

Conflicts of interest

There are no conflicts to declare.

Acknowledgements

C. Goh and A.-A.D. and acknowledge the Natural Sciences and Engineering Research Council of Canada for research funding.

References

1 M. Wu, P. Hou, L. Dong, L. Cai, Z. Chen, M. Zhao, *et al.*, Manganese dioxide nanosheets: from preparation to biomedical applications, *Int. J. Nanomed.*, 2019, **14**, 4781–4800.

2 F. Mo, G. Liang, Q. Meng, Z. Liu, H. Li, J. Fan, *et al.*, A flexible rechargeable aqueous zinc manganese-dioxide battery working at −20 °C, *Energy Environ. Sci.*, 2019, **12**(2), 706–715.

3 J. Fei, Y. Cui, X. Yan, W. Qi, Y. Yang, K. Wang, *et al.*, Controlled Preparation of MnO_2 Hierarchical Hollow Nanostructures and Their Application in Water Treatment, *Adv. Mater.*, 2008, **20**(3), 452–456.

4 Z. B. Jildeh, J. Oberrländer, P. Kirchner, P. H. Wagner and M. J. Schöning, Thermocatalytic Behavior of Manganese(IV) Oxide as Nanoporous Material on the Dissociation of a Gas Mixture Containing Hydrogen Peroxide, *Nanomaterials*, 2018, **8**(4), 262.

5 C. E. Huckaba and F. G. Keyes, The Accuracy of Estimation of Hydrogen Peroxide by Potassium Permanganate Titration, *J. Am. Chem. Soc.*, 1948, **70**(4), 1640–1644.

6 K. Kai, Y. Yoshida, H. Kageyama, G. Saito, T. Ishigaki, Y. Furukawa, *et al.*, Room-Temperature Synthesis of Manganese Oxide Monosheets, *J. Am. Chem. Soc.*, 2008, **130**(47), 15938–15943.

7 Y. Yao, Z. Lin, Z. Li, X. Song, K.-S. Moon and C.-P. Wong, Large-scale production of two-dimensional nanosheets, *J. Mater. Chem.*, 2012, **22**(27), 13494–13499.

8 Z. Huang, L. Zheng, F. Feng, Y. Chen, Z. Wang, Z. Lin, *et al.*, A Simple and Effective Colorimetric Assay for Glucose Based on MnO_2 Nanosheets, *Sensors*, 2018, **18**(8), 2525.

9 Z. Huang, J. Yang, L. Zhang, X. Geng, J. Ge, Y. Hu, *et al.*, A novel one-step colorimetric assay for highly sensitive detection of glucose in serum based on MnO_2 nanosheets, *Anal. Methods*, 2017, **9**(29), 4275–4281.

10 M. C. Y. Chang, A. Pralle, E. Y. Isacoff and C. J. Chang, A Selective, Cell-Permeable Optical Probe for Hydrogen Peroxide in Living Cells, *J. Am. Chem. Soc.*, 2004, **126**(47), 15392–15393.

11 G. Luka, A. Ahmadi, H. Najjaran, E. Alocilja, M. Derosa, K. Wolthers, *et al.*, Microfluidics Integrated Biosensors: A Leading Technology towards Lab-on-a-Chip and Sensing Applications, *Sensors*, 2015, **15**(12), 30011–30031.

12 R. Bateman and J. Evans, Using the Glucose Oxidase/Peroxidase System in Enzyme Kinetics, *J. Chem. Educ.*, 1995, **72**(12), A240–A241.

13 L. Zhao, J. Li, X. Chen, D. Cheng, J. Zhang and H. Yang, Highly sensitive electrochemical detection of hydrogen peroxide based on polyethyleneimine-Au nanoparticles-zinc protoporphyrin, *J. Electrochem. Soc.*, 2019, **166**(8), B631.

14 A. Mannaï, S. Saidi, F. Gmati and A. B. Mohamed, Effects of hydrogen peroxide on the electrical conductivity of graphite/polyaniline composites, *Mater. Sci. Semicond. Process.*, 2016, **41**, 350–357.

15 S. V. Kanth, R. Venba, B. Madhan, N. K. Chandrababu and S. Sadulla, Cleaner tanning practices for tannery pollution abatement: Role of enzymes in eco-friendly vegetable tanning, *J. Cleaner Prod.*, 2009 Mar 1, **17**(5), 507–515.

16 P. A. Caballero, M. Gomez and C. M. Rosell, Improvement of dough rheology, bread quality and bread shelf-life by enzymes combination, *J. Food Eng.*, 2007 Jul 1, **81**(1), 42–53.

17 L. H. G. van Donkelaar, J. Mostert, F. K. Zisopoulos, R. M. Boom and A.-J. van der Goot, The use of enzymes for beer brewing: Thermodynamic comparison on resource use, *Energy*, 2016, **115**(Part 1), 519–527.

18 A. Pandey, R. Singh, R. Singhania and C. Larroche, *Biomass, Biofuels and Chemicals*, Elsevier, San Diego, 2019.

19 N. R. Khan and V. K. Rathod, Enzyme catalyzed synthesis of cosmetic esters and its intensification: A review, *Process Biochem.*, 2015, **50**(11), 1793–1806.

20 D. Ercili-Cura, T. Huppertz and A. L. Kelly, Enzymatic modification of dairy product texture, in: *Modifying Food Texture* [Internet], Elsevier, 2015, pp. 71–97.

21 A. S. Meyer, Antimicrobial enzymes, in: *Food Preservation Techniques*, Elsevier, 2003, pp. 49–70.

22 C. Nick Pace, S. Trevino, E. Prabhakaran and J. Martin Scholtz, Protein structure, stability and solubility in water and other solvents, *Philos. Trans. R. Soc., B*, 2004, **359**(1448), 1225–1235.

23 C. Wang, P. Yu, Y. Wang and L. Mao, Single-Layer MnO_2 Nanosheets Suppressed Fluorescence of 7-Hydroxycoumarin: Mechanistic Study and Application for Sensitive Sensing of Ascorbic Acid in Vivo, *Anal. Chem.*, 2014, **86**(24), 12206–12213.

24 M. R. Marques, R. Loebenberg and M. Almukainzi, Simulated biological fluids with possible application in dissolution testing, *Dissolution Technol.*, 2011, **18**(3), 15–28.

25 B. E. P. Swoboda and V. Massey, *J. Biol. Chem.*, 1965, **240**, 2209–2215.

26 K. K.-A. Kim, D. R. Fravel and G. C. Papavizas, Glucose oxidase as the antifungal principle of talaron from *Talaromyces flavus*, *Can. J. Microbiol.*, 1990, **36**(11), 760–764.

 © 2021 The Author(s). Published by the Royal Society of Chemistry

Open Access Article. Published on 17 May 2021. Downloaded on 7/24/2024 3:29:31 PM.
This article is licensed under a Creative Commons Attribution 3.0 Unported Licence.

27 M. K. Jong and D. S. Rolf, *FEMS Microbiol. Lett.*, 1991, **78**, 221.
28 A. M. V. Garzillo, S. D. Paolo, M. Fenice, M. Petruccioli, V. Buonocore and F. Federici, *Biotechnol. Appl. Biochem.*, 1995, **22**, 179.
29 D. Rando, G.-W. Kohring and F. Giffhorn, Production, purification and characterization of glucose oxidase from a newly isolated strain of *Penicillium pinophilum*, *Appl. Microbiol. Biotechnol.*, 1997, **48**(1), 34–40.
30 C. Simpson, J. Jordaan, N. S. Gardiner and C. Whiteley, Isolation, purification and characterization of a novel glucose oxidase from Penicillium sp. CBS 120262 optimally active at neutral pH, *Protein Expression Purif.*, 2007, **51**(2), 260–266.
31 M.-K. Weibel and H.-J. Bright, The Glucose Oxidase Mechanism, *J. Biol. Chem.*, 1971, **246**(9), 2734–2744.
32 Y. J. Mao, X. R. Sheng and X. M. Pan, The effects of NaCl concentration and pH on the stability of hyperthermophilic protein Ssh10b, *BMC Biochem.*, 2007, **8**(1), 1–8.